5832–5844 *Nucleic Acids Research, 2021, Vol. 49, No. 10* *Published online 25 May 2021*
https://doi.org/10.1093/nar/gkab379

Dengue virus 2 capsid protein chaperones the strand displacement of 5′-3′ cyclization sequences

Xin Ee Yong [1,2], V. Raghuvamsi Palur[3], Ganesh S. Anand[3], Thorsten Wohland[2,3,*] and Kamal K. Sharma[2,3,*]

[1]NUS Graduate School Integrative Sciences and Engineering Programme, National University of Singapore, 21 Lower Kent Ridge Road, Singapore 119077, Singapore, [2]Centre for Bioimaging Sciences, National University of Singapore, 14 Science Drive 4, Singapore 117557, Singapore and [3]Department of Biological Sciences, National University of Singapore, 14 Science Drive 4, Singapore 117543, Singapore

Received January 18, 2021; Revised April 21, 2021; Editorial Decision April 26, 2021; Accepted April 28, 2021

ABSTRACT

By virtue of its chaperone activity, the capsid protein of dengue virus strain 2 (DENV2C) promotes nucleic acid structural rearrangements. However, the role of DENV2C during the interaction of RNA elements involved in stabilizing the 5′-3′ panhandle structure of DENV RNA is still unclear. Therefore, we determined how DENV2C affects structural functionality of the capsid-coding region hairpin element (cHP) during annealing and strand displacement of the 9-nt cyclization sequence (5CS) and its complementary 3CS. cHP has two distinct functions: a role in translation start codon selection and a role in RNA synthesis. Our results showed that cHP impedes annealing between 5CS and 3CS. Although DENV2C does not modulate structural functionality of cHP, it accelerates annealing and specifically promotes strand displacement of 3CS during 5′-3′ panhandle formation. Furthermore, DENV2C exerts its chaperone activity by favouring one of the active conformations of cHP. Based on our results, we propose mechanisms for annealing and strand displacement involving cHP. Thus, our results provide mechanistic insights into how DENV2C regulates RNA synthesis by modulating essential RNA elements in the capsid-coding region, that in turn allow for DENV replication.

INTRODUCTION

Like all flaviviruses, dengue virus (DENV) is an enveloped, non-polyadenylated positive-strand RNA virus with a type 1 cap structure located at the 5′ end of the genome and 5′ and 3′ untranslated regions (UTRs) flanking a single open reading frame (ORF) (1). DENV causes dengue fever and its more severe and potentially lethal manifestations, dengue hemorrhagic fever/dengue shock syndrome. The four serotypes of DENV (DENV1–4) are transmitted to humans via two mosquito species: *Aedes aegypti* or Aedes albopictus and are the leading cause of arboviral diseases worldwide (2,3). The DENV2 replication cycle begins when the virus binds and enters a susceptible host cell by receptor-mediated endocytosis, leading to the release of the viral genome into the cytoplasm. The DENV2 ORF is subsequently translated as a polyprotein from a start codon located at the 5′ end of the region encoding the viral capsid protein (DENV2C). The polyprotein is cleaved into three structural (envelope [E], pre-membrane [prM] and capsid [DENVC]) and seven non-structural proteins (NS1, NS2A, NS2B, NS3, NS4A, NS4B and NS5). The genomic RNA (vRNA) is synthesized by the viral replicase complex via a negative-sense intermediate and newly transcribed vRNA undergo late rounds of translation that are dependent upon RNA synthesis.

The 5′UTR of DENV2 contains several conserved *cis*-acting RNA elements that play a key role in regulating viral translation and RNA synthesis (3–6). The 5′ cyclization sequence (5CS) regulates RNA synthesis through interaction with the complementary 3CS located within the 3′UTR (7,8) (Figure 1A). The downstream AUG region (DAR) was identified with 5DAR located just downstream of the initiating AUG and the complementary 3DAR found in the 3′UTR (9,10). 5DAR/3DAR acts together with 5CS/3CS and the 5′/3′ upstream AUG region (5UAR/3UAR) to circularize vRNA (Figure 1A), which is a requirement for efficient RNA synthesis but is not involved in viral translation (5,8–11). Other elements involved in genome rearrangement could be located at the 5′ end, such as the downstream of 5′ cyclization sequence pseudoknot (DCS-PK) (12) or at the 3′ end, such as the pseudoknot (PK) element formed within the dumbbell structure DB2 (13).

*To whom correspondence should be addressed. Tel: +65 82906620; Email: dbskks@nus.edu.sg
Correspondence may also be addressed to Thorsten Wohland. Tel: +65 65161248; Fax: +65 67767882; Email: twohland@nus.edu.sg
Present address: Ganesh S. Anand, Department of Chemistry, Penn State University, University Park, PA 16802, Pennsylvania, USA.

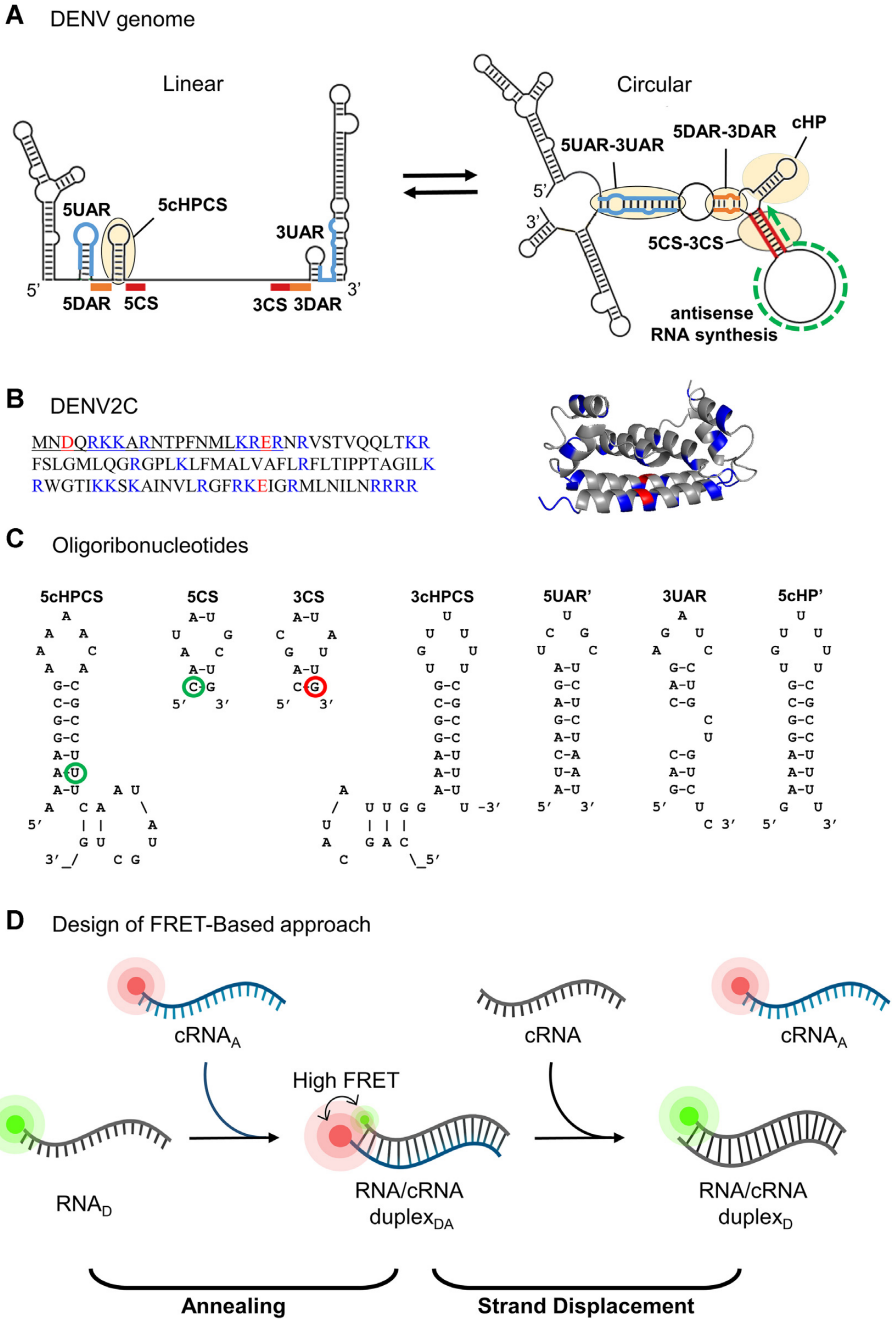

Figure 1. Schematic representation of DENV genome, DENV2C, ORN sequences and FRET-based annealing and strand displacement approach used in this study. (**A**) Switch between two conformations of DENV genome during 5′-3′ panhandle formation. The 5′ and 3′ UTR region of DENV genome contain conserved sequences: 5CS and 3CS (red blocks), 5DAR and 3DAR (orange blocks), and 5UAR and 3UAR (blue lines). 5CS is downstream of the cHP region (yellow oval in linear genome) and is an essential, sequence-independent hairpin. Annealing of conserved sequences (5CS/3CS, 5DAR/3DAR and 5UAR/3UAR) allow the formation of the circularized genome. On the other hand, the synthesis of antisense DENV RNA (green arrow) leads to strand displacement of 5CS and 3CS. (**B**) DENV2C amino acid sequence and structure (PDB: 1R6R). The DENV2C protein is a homodimer with both basic (blue) and acidic (red) residues. In the protein sequence of DENV2C monomer, the first 21 residues constitute the N-terminus disordered region (underlined). (**C**) Oligoribonucleotides. ORN sequences are derived from the 5′UTR and 3′UTR regions of the genome. Their secondary structures were predicted using the mfold webtool (http://unafold.rna.albany.edu/). 5cHPCS and 5CS are labelled with FAM as donor at the 21st position and 5′ end, respectively (green circles) while 3CS is labelled with TAMRA as acceptor at 3′ end (red circle). (**D**) Schematic representation of the FRET-Based approach. The annealing of RNA_D-$cRNA_A$ will lead to the formation of a duplex that is labelled with both FAM (green) and TAMRA (red). Due to the close proximity of donor and acceptor dyes, a high FRET efficiency and a decrease in the FAM intensity is observed. The addition of cRNA during the strand displacement reaction led to the displacement of $cRNA_A$, which shifts the two dyes apart from each other, resulting in a decrease in FRET efficiency and the restoring of FAM fluorescence.

A *cis*-acting RNA secondary structure, termed capsid-coding hairpin (cHP) (Figure 1A), was found to regulate both viral translation and RNA synthesis in a sequence-independent manner (14,15). How cHP influences DENV RNA synthesis is still unknown. cHP briefly stalls the scanning initiation complex over the first AUG, favouring its recognition (15) in the absence of a strong initiation context. When 5CS and 3CS have annealed, cHP has a stretched-out stem structure that includes the first nucleotide (nt) of 5CS (16) (5cHPCS in Figure 1A). Once the vRNA has switched from its role as an mRNA to a template for (−) RNA synthesis, cyclization decreases the length of the cHP stem slightly in the presence of the 3′UTR (16,17) (shown by 5cHPCS in Figure 1A). We hypothesize that cHP stabilizes the overall 5′-3′ panhandle structure (14,15) of DENV vRNA during (−) RNA synthesis, probably via an interplay between annealing and unpairing/strand displacement of 5CS and 3CS (Figure 1A). The annealing of conserved sequences such as 5CS and consequently, cHP and CS, in association with other cyclization motifs (DAR and UAR), could regulate DENV vRNA conformations via both annealing and strand displacement (9). This switch of DENV vRNA from circular to linear conformations modulates RNA synthesis (18).

In addition, it is believed that proteins like NS5 and NS3 helicase assist this conformational switch of DENV vRNA by unwinding secondary/tertiary structures and displacing the double-stranded (ds) regions in vRNA (19,20). This essential strand displacement process takes place during (−) RNA synthesis. Unwinding of the RNA structures and displacement of the non-template strand provides NS5 RNA-dependent RNA polymerase (RdRp) with access to the template strand (1). As the new RNA strand forms, it anneals with the template strand. Thus, two forms of genome rearrangement take place during strand displacement: unwinding and annealing. We have shown that DENV2C modulates the annealing and melting of the RNA elements in 5′UTR region of DENV2 vRNA and plays a role in genomic rearrangements (21). DENV2C is an RNA chaperone, shown to promote the annealing of the hammerhead ribozyme to its substrate as well as the dissociation of the cleaved substrates (22). As an RNA chaperone, DENV2C helps to prevent the misfolding of RNA by allowing RNA to sample many different conformations (23). DENV2C exists as a homodimer, consisting of two 100-aa subunits (Figure 1B). The protein is highly basic and has a flexible disordered region in the N-terminus, both key characteristics of many RNA chaperones (24–27). The protein associates with vRNA to form the nucleocapsid, and the nucleocapsid is encapsulated in a lipid bilayer containing E and M proteins (28). DENV2C binds to vRNA via its basic residues in helix-4 and binds to the lipid bilayer using its hydrophobic cleft in helix-1 (29,30). Considering the chaperone activity of DENV2C, we hypothesize that this protein plays a significant role both in annealing and strand displacement of 5CS and 3CS during stabilization of the 5′-3′ panhandle structure by modulating cHP (14,15).

Since cHP regulates RNA synthesis in a sequence-independent manner (14), we investigated the structural functionality of cHP during annealing and strand displacement kinetics of 9-nt 5CS to its complementary 3CS (Figure 1C). We monitored annealing kinetics using either 32-nt 5cHPCS or 9-nt 5CS, labelled with 6-carboxyfluorescein (FAM) as the donor fluorophore (Figure 1C), to the complementary 3CS labelled with carboxytetramethylrhodamine (TAMRA) as the acceptor (Figure 1C), forming a Förster resonance energy transfer (FRET) pair. With the addition of acceptor-labelled complementary 3CS to donor-labelled 5cHPCS or 5CS, the proximity between donor and acceptor dyes increases and leads to the quenching of the donor fluorescence during real-time annealing kinetics (Figure 1D). Likewise, we monitored strand displacement of acceptor-labelled 3CS from these annealed 5cHPCS/3CS or 5CS/3CS duplexes by adding excess concentrations of non-labelled 3CS that leads to fluorescence recovery of the donor (Figure 1D). By monitoring the annealing kinetics of 5cHPCS and 5CS with 3CS, we found that the presence of cHP impedes the annealing between 5CS and 3CS. However, no strand displacement was observed in both annealing complexes. Interestingly, DENV2C accelerates both 5cHPCS/3CS and 5CS/3CS annealing and promotes strand displacement of 3CS from both annealed duplexes. Moreover, we observed that DENV2C specifically nucleates the strand displacement of 3CS without disturbing the structural functionality of cHP. We also determined, using time-resolved FRET (trFRET), that DENV2C exerts its chaperoning activity by favouring one of the active conformations of 5cHPCS/3CS and 5CS/3CS duplexes. We further proposed mechanisms for 5cHPCS/3CS and 5CS/3CS annealing as well as DENV2C-promoted 3CS-strand displacement from these annealed complexes using a coupled annealing and strand displacement approach (Figure 1D). Overall, our results suggest a reaction mechanism where cHP stabilizes the 5′-3′ panhandle. In addition, we also determined how DENV2C modulates the role of cHP during 5CS-3CS annealing as well as during strand displacement. Therefore, our results improve the understanding of *cis*-acting RNA elements and reveal that DENV2C is likely to regulate RNA synthesis through the stabilization and genomic rearrangements of the essential RNA elements in the capsid-coding region that regulate DENV fitness.

MATERIALS AND METHODS

Oligoribonucleotides

All oligoribonucleotides (ORNs) were synthesized by Integrated DNA Technologies (Singapore). Donor-labelled 5cHPCS and 5CS were synthesized with 6-carboxyfluorescein (FAM) at the 21st position and the 5′ end, respectively (Figure 1C). Acceptor-labelled 3CS were synthesized with carboxytetramethylrhodamine (TAM) at the 3′ end (Figure 1C). All ORNs were purified by the manufacturer using HPLC.

DENV2C protein synthesis and purification

DENV2C protein was expressed and purified as described in an earlier study (21). DENV2C protein preparations were ribonuclease- (21) and RNA-free, determined by a A_{260}/A_{280} value of 0.7 for the purified protein, very close to

the theoretical value of 0.57 for a protein sample not contaminated by nucleic acids.

Fluorescence spectroscopy

Fluorescence spectroscopy measurements were done on a Cary Eclipse Fluorescence Spectrophotometer (Agilent) with a temperature control module, using Hellma® fluorescence cuvettes with an internal chamber volume of 45 μl. Excitation and emission wavelengths of 480 and 520 nm were used to track the intensity of FAM in real-time. Annealing reactions were performed in second order conditions by adding acceptor-labelled ORN to donor-labelled ORN at a 1:1 ratio while the strand displacement reactions were performed in pseudo first-order conditions with the concentration of non-labelled ORN being at least 10-fold more than the doubly labelled annealed complexes. Equal volumes of both reactants were mixed at the start of the reaction to prevent high local concentrations of either reactant. A final concentration of 2 μM DENV2C was used for monitoring the effect of DENV2C either on annealing or on strand displacement reactions. All reactions were performed in 50 mM HEPES, 30 mM NaCl, 0.2 mM $MgCl_2$, pH 7.5 buffer and at 20°C. Reactions at high complementary ORN concentrations could not be monitored reliably at higher temperatures (>20°C) as they were too fast. All curve fitting was done on OriginProTM software (ver 9.55).

Time-resolved FRET (trFRET)

Time-resolved FRET (trFRET) measurements were carried out on a commercial Olympus FV1200 laser scanning confocal microscope equipped with a time-resolved LSM upgrade kit (Microtime 200, PicoQuant, GmbH, Berlin, Germany). Donor-labelled ORNs were excited with a 485 nm pulsed diode laser with a 20 MHz repetition rate and 29 mW power (PDL series, Sepia II combiner module). The beam was focused into the sample by a water immersion objective (60 ×, NA 1.2; Olympus, Singapore) after being reflected by a dichroic mirror (DM405/485/543/635, Olympus, Singapore) and the scanning unit. The fluorescence was collected by the same objective followed by a pinhole (120 mm) to remove out-of-focus light. The fluorescence signal was spectrally divided into donor (green) and acceptor (red) channels by a 560 DCLP mirror. The FAM donor fluorescence was recorded by a SPAD (SPCM-AQR-14, PerkinElmer Optoelectronics, Quebec, Canada) through a 513/17 band pass emission filter (Omega, VT). This donor signal was further processed by a time correlated single photon counting card (TimeHarp 260, PicoQuant) to build up the histogram of photon arrival times. The trFRET measurements were recorded for 180 s at 20°C. The mean lifetime (τ) was calculated from the individual fluorescence lifetimes (τ_i) and their relative amplitudes (a_i) according to $(\tau) = \sum \alpha_i \tau_i$. Donor fluorescence lifetime decay data were treated using the software SymPhoTime 64 (PicoQuant, GmbH). In all cases, χ^2 values were close to 1 and weighted residuals as well as their autocorrelation were distributed randomly around 0, indicating a good fit. The reported values are mean and standard deviations from at least three replicates.

RESULTS

5CS/3CS annealing is 2-fold faster in the absence of cHP

We monitored annealing kinetics of donor-labelled 5cHPCS to its complementary acceptor-labelled 3CS by tracking the decrease in FAM fluorescence (Figure. 2A). Comparing the emission spectra of donor-labelled 5cHPCS at the start and end of the annealing reaction shows an increase in FRET with the formation of the duplex that contains both FAM and TAMRA in close proximity, as seen by a decrease in FAM fluorescence (Supplementary Figure S1). The real-time fluorescence intensity traces of the 5cHPCS/3CS reaction kinetics were fitted to a mono-exponential equation (1), where $I(t)$ is the fluorescence intensity at 520 nm, upon excitation at 480 nm, k_{obs} is the second order reaction rate and t_0 is the start time of the reaction. I_0 and I_f are the fluorescence intensities of donor-labelled 5cHPCS where the 5CS region is single-stranded (in the absence of acceptor-labelled 3CS) or in the double-strand duplex form due to the presence of acceptor-labelled 3CS, respectively.

$$I\ (\mathrm{t}) = I_f\ - (I_f - I_0)\left(e^{(-k_{obs}(t-t0))}\right) \quad (1)$$

The reaction rates, k_{obs}, were plotted against the concentrations of acceptor-labelled 3CS and were observed to vary linearly with increasing 3CS concentration ([3CS]) (Figures 3A and 2B). The linear relationship between k_{obs} and [3CS] follows equation (2) (30–32).

$$k_{obs} = k_{ass}\ [3CS] + k_{diss} \quad (2)$$

Fitting the linear plot of k_{obs} against increasing [3CS] with equation (2) generated kinetic parameters shown in Table 1. Based on the acquired kinetic parameters and a continuous decrease in donor intensity plateau with increasing [3CS] (Figure 2B), a reaction mechanism with a single kinetic pathway can be proposed:

Where the final stable extended duplex, 5cHPCS/3CS, is formed through a bimolecular reaction (32,33). The formation of the 5cHPCS/3CS duplex is governed by the second order association constant, k_{ass}, and the first order dissociation constant, k_{diss}, respectively. We obtained the k_{ass} value of 66.3 (± 3) × 10^3 $M^{-1}s^{-1}$ and the k_{diss} value of 23.4 (± 2.8) × 10^{-4} s^{-1} for 5cHPCS/3CS annealing (Table 1). Since k_{ass} value is at least two orders of magnitude smaller than the rate constants reported for annealing of unstructured sequences (10^5–10^7 $M^{-1}s^{-1}$), it seems that the 5CS region of 5cHPCS undergoes structural rearrangement during the formation of the extended duplex in the presence of complementary 3CS. We validate the postulated annealing mechanism (34–37) using the numerical resolution software Dynafit (38), which allows simultaneous fitting of experimental real-time progress curves obtained at different [3CS] (Supplementary Figure S2). The estimated elementary rate constants k_{ass} and k_{diss} (Supplementary Table S1) were in excellent agreement with our experiments (Table 1) and validated the proposed annealing mechanism for the 5cHPCS/3CS reaction.

Similar to 5cHPCS/3CS annealing, 5CS/3CS annealing showed a linear dependence of the k_{obs} values (Figure 3B) as well as a continuous decrease in donor intensity plateau

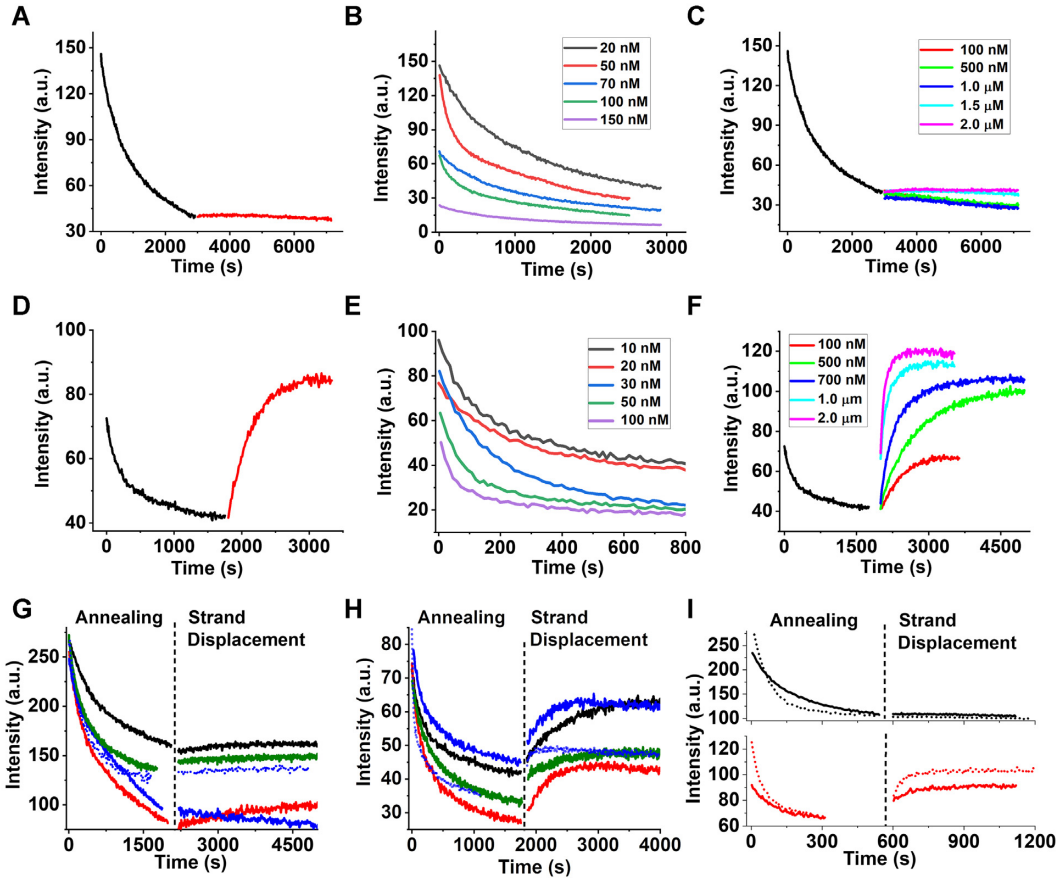

Figure 2. Real-time progress curves of 5cHPCS/3CS annealing and 5cHPCS/3CS' strand displacement in the absence (**A–C**) and presence (**D–F**) of DENV2C, and the effect of NaCl, $MgCl_2$, and temperature on annealing and strand displacement (**G–I**). Progress curves of 10 nM FAM-labelled 5cHPCS annealing (black traces) with 10 nM TAMRA-labelled 3CS and strand displacement (red traces) with 300 nM non labelled 3CS in the (A) absence and (D) presence of DENV2C. Progress curves of 10 nM FAM-labelled 5cHPCS/3CS annealing with increasing concentration of TAMRA-labelled 3CS in (B) absence and (E) presence of 2 μM DENV2C. The concentration of 3CS added is shown in the legend. Progress curves of 5cHPCS/3CS' strand displacement initiating from the duplex formed during 5cHPCS/3CS annealing in (C) absence and (F) presence of DENV2C at various concentrations of 3CS' (concentration shown in legend). All annealing and strand displacement traces were fitted using equation (1) and the obtained values are provided in Figure 3. Excitation and emission wavelengths used were 480 and 520 nm, respectively. (**G** and **H**) Effect of NaCl and $MgCl_2$ on annealing and strand displacement in (G) absence and (H) presence of DENV2C. 5cHPCS/3CS annealing was performed using 10 nM FAM 5cHPCS and 10 nM TAMRA-labelled 3CS, followed by 5cHPCS/3CS' strand displacement with 100 nM non-labelled 3CS' in different buffer conditions to observe the effect of NaCl and $MgCl_2$ (solid traces). 5CS/3CS annealing was performed using 10 nM FAM-labelled 5CS and 10 nM TAMRA-labelled 3CS, followed by 5CS/3CS' strand displacement with 100 nM non-labelled 3CS' in different buffer conditions to observe the effect of NaCl and $MgCl_2$ (dotted traces). All annealing and strand displacement traces were fitted with equation (1) and k_{obs} values are provided in Table 3. (**I**) Effect of temperature on annealing and strand displacement in absence (black traces) and presence (red traces) of DENV2C. 5cHPCS/3CS annealing was performed at 37°C using 10 nM FAM 5cHPCS and 10 nM TAMRA-labelled 3CS followed by 5cHPCS/3CS' strand displacement with 100 nM non-labelled 3CS' (solid traces). 5CS/3CS annealing was performed at 37°C using 10 nM FAM 5CS and 10 nM TAMRA-labelled 3CS followed by 5CS/3CS' strand displacement with 100 nM non-labelled 3CS' (dotted traces). Fitting of annealing and strand displacement traces with equation (1) provided k_{obs} values in Table 4.

against increasing [3CS], indicating a similarity of reaction mechanism to that proposed by Scheme 1 (shown by Scheme Sa in the Supplementary Data). The 5CS/3CS annealing reaction was found to be ∼2-fold faster as compared to the 5cHPCS/3CS annealing reaction (by comparing corresponding k_{ass} values in Table 1), indicating a hindrance in 5cHPCS/3CS annealing due to the presence of cHP. cHP serves only a structural function in 5cHPCS/3CS annealing, and yet it seems to modulate the annealing of 5CS to its complementary 3CS. On the other hand, similar values of k_{diss} for both 5cHPCS/3CS and 5CS/3CS annealing suggest that cHP has a limited effect on the stability of 5CS-3CS duplex formation (Table 1).

DENV2C accelerates both 5cHPCS/3CS and 5CS/3CS annealing

Since DENV2C has been shown to chaperone annealing of essential RNA elements (UAR and cHP) from the DENV2 5′UTR region (21), we investigated if DENV2 chaperones the annealing of 5cHPCS/3CS and 5CS/3CS and whether it alters the hindering effect of cHP. We mimicked large molecular ribonucleoprotein (RNP) complex conditions (39–41) by using DENV2C at a DENV2C:ORN molar ratio of 100:1 (Supplementary Figure S3A) to characterize the annealing of 5cHPCS/3CS and of 5CS/3CS. Addition of DENV2C to donor-labelled 5cHPCS and 5CS led to a decrease in their fluorescence (compare black emission spectra

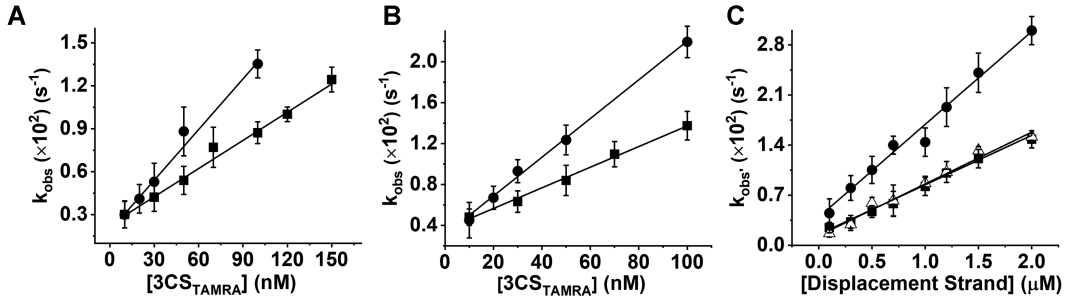

Figure 3. Kinetic parameters of (**A**) 5cHPCS/3CS and (**B**) 5CS/3CS annealing and (**C**) 5cHPCS/3CS', 5CS/3CS' and 5cHPCS/3cHPCS strand displacement in the absence and presence of DENV2C. Kinetic parameters were obtained by fitting real-time progress curves shown in Figure 2. During (A) 5cHPCS/3CS and (B) 5CS/3CS annealing, the obtained values of apparent rates (k_{obs}) were plotted against increasing concentrations of the complementary TAMRA-labelled 3CS in (squares) absence and (circles) presence of DENV2C. (**C**) Kinetic rates ($k_{obs'}$) for the displacement of TAMRA-labelled 3CS during 5cHPCS/3CS' (squares), 5CS/3CS' (circles) and 5cHPCS/3cHPCS (open triangles) were also plotted against increasing concentration of displacement strands (3CS' and 3cHPCS). All plotted kinetic rates were fitted to equation (2) and the obtained values are provided in Table 1. Excitation and emission wavelengths used were 480 and 520 nm, respectively. Error bars show standard deviation from at least three repeats.

Table 1. Kinetic parameters of 5cHPCS/3CS and 5CS/3CS annealing, and 5cHPCS/3CS', 5CS/3CS' and 5cHPCS/3cHPCS strand displacement in the absence and presence of DENV2C. Kinetic rate constants, k_{ass}, k_{diss}, $k_{ass'}$ and $k_{diss'}$, were calculated from the dependence of the k_{obs} values on the concentration of the non-labelled ORN, using equation (2) as indicated in Figure 3

		Annealing[a]			Strand displacement[b]		
Fluorescein-labelled ORN	TAMRA-labelled complementary ORN	DENV2C (μM)	k_{ass} ($M^{-1}s^{-1}$) $\times 10^{-3}$	k_{diss} (s^{-1}) $\times 10^4$	Non-labelled strand displacement ORN	$k_{ass'}$ ($M^{-1}s^{-1}$) $\times 10^{-3}$	$k_{diss'}$ (s^{-1}) $\times 10^4$
5cHPCS	**3CS**	0	66.3 (±3)	23.4 (±2.8)	**3CS'**	-	-
5CS	**3CS**	0	102.4 (±5)	35.2 (±3)	**3CS'**	-	-
5cHPCS	**3CS**	2	119.2 (±8)	19.4 (±4)	**3CS'**	6.8 (±0.2)	14.4 (±2.5)
5cHPCS	**3CS**	2			**3cHPCS**	7.3 (±0.4)	12.9 (±4.5)
5CS	**3CS**	2	193 (±7)	28.4 (±3)	**3CS'**	13.3 (±0.4)	35.5 (±5.5)

[a]Annealing reactions were performed in second-order reaction conditions with both annealing partners at 10 nM concentrations.
[b]Strand displacement reactions were performed in pseudo-first order conditions by adding non-labelled 3CS or 3cHPCS at least 10-fold molar excess of the annealed duplex.

$$5cHPCS + 3CS \underset{k_{diss}}{\overset{k_{ass}}{\rightleftharpoons}} 5cHPCS/3CS$$

Scheme 1.

in Supplementary Figure S1A and S1B, respectively), indicating the condensation of RNA sequences due to the binding of DENV2C with ORNs in RNP complex conditions (39–41). Annealing of 5cHPCS/3CS and of 5CS/3CS were then triggered by adding acceptor-labelled 3CS to the preformed complex of either 5cHPCS or 5CS and DENV2C (Figure 2D). The real-time fluorescence intensity traces of both DENV2C-promoted 5cHPCS/3CS (Figure 2D) and 5CS/3CS (Supplementary Figure S3C) showed mono-exponential decreases in FAM intensity and were fitted with equation (1). Both DENV2C-promoted 5cHPCS/3CS and 5CS/3CS annealing showed a linear dependence of the k_{obs} values, as well as a continuous decrease in donor intensity plateau with increasing [3CS] (Figure 3A and B). Thus, a similar reaction mechanism to that proposed by Scheme 1 can be suggested. As expected, DENV2C accelerated both 5cHPCS/3CS and 5CS/3CS annealing, and a ∼2-fold increase in k_{obs} in the presence of DENV2C was observed when compared to the corresponding annealing in the absence of the protein (Table 1). Incidentally, DENV2C-promoted 5CS/3CS annealing was still found to be ∼2-fold faster as compared to DENV2C-promoted 5cHPCS/3CS annealing (by comparing the corresponding k_{ass} values in Table 1), suggesting that DENV2C does not regulate the structural functionality of cHP in 5cHPCS/3CS annealing.

DENV2C promotes strand displacement of 3CS from both 5cHPCS/3CS and 5CS/3CS complexes

Next, we monitored strand displacement kinetics of acceptor-labelled 3CS from preformed donor/acceptor-labelled 5cHPCS/3CS and 5CS/3CS duplexes, by adding non-labelled 3CS in at least 10-fold molar excess. Due to the pseudo-first order conditions, the addition of non-labelled 3CS should displace acceptor-labelled 3CS from either the 5cHPCS/3CS or 5CS/3CS duplex leading to an increase and opposite decrease in the FAM and TAMRA fluorescence, respectively. Contrary, no changes in the strand displacement kinetic traces and the emission spectra of the dual-labelled 5cHPCS/3CS (Figure 2C and Supplementary Figure S1A) or 5CS/3CS (Supplementary Figure S3B) duplexes at the start and end of the strand displacement reaction were observed, thus suggesting that no strand displacement takes place in these conditions. We tested up to 200-fold excess non-labelled 3CS to investigate strand-displacement but could not detect any increase in FAM fluorescence suggesting the stability of both 5cHPCS/3CS or

$$\text{5cHPCS/3CS + 3CS'} \underset{k_{diss'}}{\overset{k_{ass'}}{\rightleftharpoons}} \text{5cHPCS/3CS'}$$

Scheme 2.

5CS/3CS annealed duplexes (Figure 2C and Supplementary Figure S3B). In contrast, the addition of non-labelled 3CS, even at 10-fold excess, leads to a rapid increase in FAM fluorescence in the presence of DENV2C (Figure 2D and Supplementary Figure S4B). The result proves the chaperoning role of DENV2C in the strand displacement of acceptor-labelled 3CS and thus, in aiding genomic rearrangement.

The real-time fluorescence intensity traces of DENV2C-promoted 3CS strand displacement from either the 5cHPCS/3CS (Figure 2F) or 5CS/3CS (Supplementary Figure S3C) annealed duplex were fitted to equation (1). I(t) is the actual fluorescence intensity at 520 nm, upon excitation at 480 nm, I'_0 and I'_f are the fluorescence intensities of donor/acceptor-labelled 5cHPCS or 5CS/3CS before and after completion of strand displacement reaction kinetics, respectively. t_0 is the start time of the reaction. The fitted pseudo first order reaction rate for strand transfer reactions is $k_{obs'}$.

The strand transfer reaction rates, $k_{obs'}$, were plotted against the concentration of non-labelled 3CS (Figure 3C) and were observed to linearly vary with increasing concentrations of 3CS. As mentioned earlier, the linear relationship between $k_{obs'}$ and [3CS] follows equation (2) (30–32). The obtained kinetic parameters for strand transfer reactions are $k_{ass'}$ and $k_{diss'}$.

The kinetic parameters obtained by fitting the linear plot of $k_{obs'}$ against increasing [3CS] with equation (2) are shown in Table 1. Based on the acquired kinetic parameters coupled to the continuous increase in donor intensity plateau (Figure 2F and Supplementary Figure S3C), a reaction mechanism can be proposed for both DENV2C promoted-3CS displacement from either 5cHPCS/3CS (Scheme 2) or 5CS/3CS (Scheme b in the Supplementary Data):

Where the final displaced duplex, 5cHPCS/3CS' or 5CS/3CS', is formed through a bimolecular reaction (32,33) and is governed by the second order association constant, $k_{ass'}$, and the first order dissociation constant, $k_{diss'}$, respectively. The observed values of $k_{ass'}$ and $k_{diss'}$ were 6.8 ($\pm$ 0.2) $\times$ 10^3 $M^{-1}s^{-1}$ and 14.4 ($\pm$ 2.5) $\times$ 10^{-4} s^{-1}, respectively, for 5cHPCS/3CS' strand displacement (Table 1). In addition, a comparison of the k_{ass} and $k_{ass'}$ values indicate that 5cHPCS/3CS annealing is ~20-fold faster compared to that of 5cHPCS/3CS' strand displacement. Therefore, the strand displacement events require the presence of DENV2C to chaperone the displacement of strands from the annealed ORNs complexes, in line with literature (23–27). The corresponding $k_{ass'}$ and $k_{diss'}$ values for 5CS/3CS' strand displacement were found to be 13.3 ($\pm$ 0.4) $\times$ 10^3 $M^{-1}s^{-1}$ and 35.5 ($\pm$ 5.5) $\times$ 10^{-4} s^{-1}, respectively (Table 1). Furthermore, the postulated strand displacement mechanisms for both 5cHPCS/3CS' and 5CS/3CS' were validated using Dynafit (38) by simultaneously fitting the experimental progress curves obtained at different [3CS] (Supplementary Figure S2). Again, the estimated rate constants $k_{ass'}$ and $k_{diss'}$ (Supplementary Table S1) were in excellent agreement with those found by our experiments (Table 1). Interestingly, DENV2C-promoted strand displacement of 3CS from the 5cHPCS/3CS annealed complex (5cHPCS/3CS') was found to be ~2-fold slower as compared to DENV2C-promoted 5CS/3CS' strand displacement (by comparing the corresponding $k_{ass'}$ values in Table 1), suggesting that cHP plays a structural function in modulating both annealing as well as strand displacement reactions.

DENV2C-promoted stand displacement of 3CS initiates at the 3′ end of 5cHPCS

We further characterize the molecular mechanism of 5cHPCS/3CS' strand displacement by investigating the nucleation of 3CS displacement. To determine whether 3CS is displaced at the bottom of the cHP stem or at the 3′ end of the 5cHPCS overhang, we used a 32-nt 3cHPCS RNA sequence, where 3CS is elongated by adding complementary nucleotides corresponding to the 5cHP region (Figure 1C). If 3CS displacement starts from the bottom of the cHP stem of the 5cHPCS/3CS annealed duplex, slower kinetic parameters as compared to 5cHPCS/3CS' strand displacement are expected due to presence of two cHP-like structures which need to be annealed before displacing 3CS. On the other hand, no or minimal changes in the kinetic parameters are expected if the displacement of 3CS from the 5cHPCS/3CS annealed duplex nucleates from the 3′ end of 5cHPCS, as no changes in the FAM fluorescence will be observed due to annealing of two cHP-like structures.

The real-time fluorescence intensity traces of DENV2C-promoted 3CS strand displacement from the 5cHPCS/3CS annealed duplex in the presence of increasing concentrations of 3cHPCS (Supplementary Figure S4C) were fitted to a mono-exponential equation (1). Further, the reaction rates, $k_{obs'}$, were plotted against the concentration of non-labelled 3cHPCS (Figure 3C) and were observed to be linearly varying with increasing concentration ([3cHPCS]). The linearly varying kinetic parameters coupled to the continuous increase in donor intensity plateau again suggest that the reaction mechanism is similar to that of 5cHPCS/3CS' (Scheme c in the Supplementary Data). Furthermore, the observed values of 7.3 ($\pm$ 0.4) $\times$ 10^3 $M^{-1}s^{-1}$ and 12.9 ($\pm$ 4.5) $\times$ 10^{-4} s^{-1} for $k_{ass'}$ and $k_{diss'}$ respectively for 5cHPCS/3cHPCS' strand displacement are similar to the corresponding values of 5cHPCS/3CS' (Table 1). Therefore, our results suggest that the displacement of 3CS from the 5cHPCS/3CS annealed duplexes nucleates at the 3′ end of 5cHPCS.

DENV2C specifically promotes 3CS displacement

Next, we determined the specificity of 3CS strand displacement from the 5cHPCS/3CS duplex in DENV2C-promoted 5cHPCS/3CS' strand displacement. For this, we performed strand displacement of acceptor-labelled 3CS from the 5cHPCS/3CS duplex using non-labelled 23-nt 5cHP', 21-nt 3UAR and 21-nt 5UAR' (Figure 1C). We compared the efficiency of these three sequences in displacing 3CS from the 5cHPCS/3CS annealed duplex with

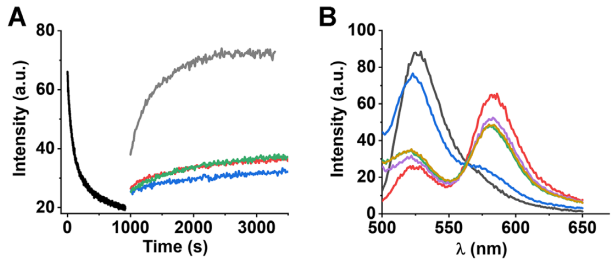

Figure 4. Specificity in the displacement of 3CS. (**A**) Real time progress curves of annealing (black trace) between 10 nM FAM-labelled 5cHPCS with 10 nM TAMRA-labelled 3CS. Strand displacement of acceptor-labelled 3CS from preformed 5cHPCS/3CS annealing duplex (black trace) in the presence of 300 nM non-labelled 3CS (grey trace), 300 nM 5cHP' (red trace), 300 nM 3UAR (blue trace) and 300 nM 5UAR' (green trace). All reactions were performed in the presence of 2 μM DENV2C. The excitation and emission wavelengths were 480 nm and 520 nm, respectively. Fitting annealing curve (black trace) with equation (1) provided $k_{obs} = 3.2 \times 10^{-3}$ s^{-1}. Fitting of strand displacement reactions with equation (1) provided values for 5cHPCS/3CS' ($k_{obs'} = 3.7 \times 10^{-3}$ s^{-1}), 5cHPCS/5cHP' ($k_{obs'} = 3.4 \times 10^{-5}$ s^{-1}), 5cHPCS/3UAR ($k_{obs'} = 3.2 \times 10^{-5}$ s^{-1}) and 5cHPCS/5UAR' ($k_{obs'} = 4.5 \times 10^{-5}$ s^{-1}). The 5cHPCS/5cHP', 5cHPCS/3UAR and 5cHPCS/5UAR' reactions were 2 orders of magnitude slower as compared to the 5cHPCS/3CS' reaction, showing the displacement of 3CS from annealed duplex. (**B**) Emission spectra of 10 nM FAM-labelled 5cHPCS before (grey) and after (red) the annealing reaction with 10 nM TAMRA-labelled 3CS. Emission spectra acquired at the end of the strand displacement reactions for 5cHPCS/5cHP' (pink), 5cHPCS/3UAR (green), 5cHPCS/5UAR' (yellow) and 5cHPCS/3CS' (blue). The excitation wavelength was 480 nm.

native non-labelled 3CS. 5cHP' is complementary to the 5cHP region of 5cHPCS. Therefore, 5cHP' should not displace acceptor-labelled 3CS due to the melting of cHP (Supplementary Figure S5). Furthermore, both 3UAR and 5UAR' show either non- or partial-complementarity to 5cHPCS and thus, should not displace acceptor-labelled 3CS if 5cHPCS/3CS' strand displacement is specific (Supplementary Figure S5). As expected, minimal to no increase in FAM fluorescence was observed upon the addition of either 5cHP', 3UAR or 5UAR' as compared to native 3CS (Figure 4A and B), suggesting that the specific complementarity between 3CS and 5CS is a requisite for DENV-promoted 5cHPCS/3CS' strand displacement.

DENV2C protein chaperones 5cHPCS/3CS and 5CS/3CS annealing and 5cHPCS/3CS' and 5CS/3CS' strand displacement by stabilizing the kinetically active duplex

We have earlier investigated the DENV2C chaperone activity during the annealing of various essential RNA elements from the 5′UTR (21). Here we focused on understanding how DENV2C chaperones 5cHPCS/3CS' and 5CS/3CS' strand displacement. For this, we investigated whether DENV2C favours any kinetically active duplex as is the case of annealing of complementary sequences (21) using trFRET. In trFRET, the energy transfer from donor to acceptor influences the donor fluorescence lifetime, τ, in a distance-dependent manner. The closer the donor and acceptor dyes are, the faster the donor dye relaxes to ground state and the shorter the lifetime. The fluorescence of 5cHPCS had an average lifetime ($<\tau_{avg}>$) of 3.8 ± 0.3 ns (Table 2) and was best fitted with two discrete lifetime components of 5.2 ± 0.3 ns ($<\tau_1>$) and 2.06 ± 0.2 ns ($<\tau_2>$), having populations of 54 ± 7% (α_1) and 46 ± 13% (α_2) respectively (Table 2). The existence of more than one population for donor-only labelled 5cHPCS indicates that FAM fluorescence in the cHP region is quenched by neighbouring nucleotides, probably due to at least two different conformations of the 5CS overhang (Supplementary Figure S6A). Moreover, we cannot exclude the existence of conformations with very short lifetimes or with lifetimes close to the two principal components, which would not be resolve in our experimental conditions. Similarly, we observed two different conformations for donor-only labelled 5CS with an average lifetime of 3.6 ± 0.6 ns (Table 2) and two discrete lifetime components of 5.13 ± 0.5 ns ($<\tau_1>$) and 2.09 ± 0.3 ns ($<\tau_2>$) having populations of 51 ± 4% (α_1) and 49 ± 9% (α_2), respectively (Table 2).

With the addition of acceptor-labelled 3CS and by forming the dual-labelled 5cHPCS/3CS duplex, the average lifetime of 5cHPCS decreased to 3.07 ± 0.4 ns (Table 2). The decay curve was best fitted with two discrete lifetime components of 5.6 ± 0.4 ns ($<\tau_1>$) and 1.3 ± 0.4 ns ($<\tau'_2>$), having populations of 40 ± 5% (α_1) and 60 ± 13% (α'_2), respectively (Table 2). The similarity between the values of $<\tau_1>$ for the 5cHPCS/3CS duplex (∼5.6 ns) and for 5cHPCS in the absence of acceptor-labelled 3CS (∼5.2 ns) probably indicates that this lifetime corresponds to the free form of 5cHPCS. Consequently, a corresponding decrease in the values of the second discrete lifetime ($<\tau_2> = 2.06$ ns vs $<\tau'_2> = 1.3$ ns) suggests the existence of 5cHPCS in hybridized/annealed form. Their corresponding populations are shown as α_1 and α'_2 (Table 2). A similar result was obtained with the addition of acceptor-labelled 3CS to donor-labelled 5CS, indicating similarities to the 5CS-3CS duplex (Table 2). Interestingly, an additional 7–9% increase in duplex formation was observed, when annealing of 3CS with 5cHPCS or 5CS occurred in the presence of DENV2C. This increase of duplex formation takes place probably at the expense of conformations that were not annealed. The trFRET results suggest that DENV2C exerts its RNA chaperone function during both annealing and strand displacement by increasing, as well as stabilizing the kinetically active double stranded 5cHPCS/3CS or 5CS/3CS duplexes.

DISCUSSION

Coding-region elements that are required for RNA synthesis have been characterized in other positive-strand viruses like human rhinovirus-14 and human rhinovirus-2 (HRV-14 and HRV-2) (42–44), poliovirus (45), coxsackievirus B3 (46) and encephalomyocarditis viruses (47). In all viruses, these elements are found to be essential for viral RNA synthesis (43,46–49). Within the *Flaviviridae* family, Hepatitis C Virus (HCV) features similar internal structure located near the 3′ end of the genome in the NS5B-coding region (50,51). A number of *cis* elements in the UTRs of flavivirus genomes have been shown to perform multiple roles in the viral life cycle (5–7,49–59). cHP is the first element in the flavivirus coding region for which two distinct functions have been characterized: a role in translation start codon selection (15) and a role in RNA synthesis (14). As a replication element, cHP performs in a sequence-

Table 2. Lifetime parameters of 5cHPCS, 5cHPCS/3CS, 5CS and 5CS/3CS duplexes in the absence and presence of DENV2C. The lifetime traces for single-labelled ORN (5cHPCS and 5CS) and dual-labelled duplex (5cHPCS/3CS and 5CS/3CS) were fitted to the bi-exponential decay model, and the average fluorescence lifetimes ($<\tau_{avg}>$) of FAM for donor were calculated in the absence and presence of DENV2C. Fitting of the fluorescence decay provided two discrete lifetimes, $<\tau_1>$ and $<\tau_2>$ with the corresponding fraction of each population as α_1 and α_2, respectively. Fitting of the fluorescence decay of FAM in the presence of acceptor (TAMRA) labelled ORN sequences provided two discrete lifetimes, $<\tau_1>$ and $<\tau_2'>$ with the corresponding fraction of each population as α_1 and α'_2, respectively. For lifetime traces in the presence of DENV2C, the protein was added at molar concentration of 2 μM, as indicated in material and methods section. Error bars represents standard deviations of at least three repeats

ORN	$<\tau_{avg}>$ (ns)	α_1 (%)	α_2 (%)	α'_2 (%)	$<\tau_1>$ (ns)	$<\tau_2>$ (ns)	$<\tau'_2>$ (ns)
5cHPCS	3.8 (±0.3)	54 (±7)	46 (±13)		5.21 (±0.3)	2.06 (±0.2)	
5cHPCS/3CS	3.07 (±0.4)	40 (±5)		60 (±7)	5.64 (±0.4)		1.33 (±0.4)
5cHPCS/3CS + DENV2C	2.6 (±0.2)	33 (±8)		67 (±6)	5.36 (±0.2)		1.24 (±0.1)
5CS	3.64 (±0.6)	51 (±4)	49 (±9)		5.13 (±0.5)	2.09 (±0.3)	
5CS/3CS	3.03 (±0.2)	40 (±10)		60 (±5)	5.57 (±0.4)		1.32 (±0.3)
5CS/3CS + DENV2C	2.6 (±0.3)	29 (±10)		71 (±10)	5.32 (±0.6)		1.40 (±0.4)

independent manner, which implies that the overall topology of the 5′ end and selection of the first codon by the scanning ribosome are important for promoting RNA synthesis. Moreover, in promoting RNA synthesis, these replication elements could allow for various conformations of vRNA as sequences anneal and melt. One such conformational large-scale genome rearrangement is the 5′-3′ panhandle formation during vRNA cyclization and its melting during vRNA linearization. Therefore, investigating the annealing and strand displacement mechanism of specific *cis* elements like cHP and CS would extract information about the function of cHP during RNA synthesis.

In this study, we have shown using both annealing and strand displacement kinetics that the presence of 5cHP modulates both annealing as well as strand displacement of 3CS to and from the 5CS region. trFRET data showed that 5cHPCS exists in two different conformations (Supplementary Figure S6A), of which one conformation is probably the more kinetically active structure, allowing annealing and strand displacement to occur. Although we observed that 5cHP modulates the annealing of 5CS to its complementary 3CS, no strand displacement was observed, thus specifying the need for RNA chaperones.

RNA chaperones like DENV2C are vital in preventing RNA misfolding by allowing RNA to escape unfavourable kinetic conformations (21,23,34–35,60–66). Therefore, we characterized the role of DENV2C by investigating the annealing and strand displacement kinetics of 5cHPCS and 5CS to complementary 3CS. Due to its chaperone properties, DENV2C accelerates 5cHPCS/3CS annealing while inducing the 5cHPCS/3CS' strand displacement reaction. Our results also showed that DENV2C specifically nucleates strand displacement of the 3CS without disturbing the structural functionality of the cHP hairpin. Overall, DENV2C-promoted annealing coupled with strand displacement occurs via a favoured active conformation of 5cHPCS, where the 5CS region is probably unstructured (compare 5cHPCS and $5cHPCS_1$ in Figure 5). The population of this conformation increases from ∼46% to ∼67% in the presence of DENV2C. Since DENV2C does not melt the stem region of 5cHP (21), this reactive species of 5cHPCS probably arises from the melting of C_{23}-G_{32} and A_{24}-U_{31} base pairs in 5CS (Figure 5 and Supplementary Figure S6B). This DENV2C-promoted reactive species (5cHPCS in Figure 5) probably led to an enhanced annealed product formation from ∼16% to ∼30% in our working conditions (Supplementary Figure S6C). In addition, the incremental annealed product formation with increasing concentration of [3CS] led to the continuous decrease in the donor intensity plateau (Figure 2B and E). Interestingly, the ∼2-fold increase in annealed product formation (Supplementary Figure S6C) correlates well with a similar increase in the DENV2C-promoted kinetic rates (compare k_{ass} values in Table 1).

The strand displacement event resulting in an RNA duplex caused by a third, invading RNA molecule relates to the process of RNA annealing. RNA chaperones destabilize double strands, starting from the ends or bulges of the base-paired region, independent of the thermodynamic stability of the double strand (67). A third strand can utilize such destabilized regions as starting points for invasion (Figure 5). The concerted process of opening the initial double strand and of annealing the new duplex finally results in either the replacement of the original strand (3CS) or the expulsion of the invading strand (3CS'), according to the kinetic and thermodynamic conditions. We observed that DENV2C could catalyse strand displacement either by destabilizing edges or by favouring annealing of the invading strand. Therefore, the proposed mechanism for DENV2C-promoted 3CS strand displacement from the 5cHPCS/3CS duplex propagates through the formation of an intermediate triplex (5cHPCS/3CS-3CS' complex in Figure 5). This intermediate triplex originates due to the nucleation of 3CS strand displacement from the 5cHPCS/3CS duplex via the 3′ end of 5cHPCS (Figure 5) and the subsequent displacement of acceptor-labelled 3CS. However, the complete displacement of 3CS from the 5cHPCS/3CS annealed duplex probably takes place only at ∼200-fold excess of displacing sequences ([3CS'] and [3cHPCS]) (Supplementary Figure S6D). Similarly, a reaction mechanism is proposed for DENV2C-promoted coupled annealing and strand displacement of 5CS with its complementary 3CS (Supplementary Figure S7).

We analysed the effect of higher ion (Na^+ and Mg^{2+}) concentration and temperature (37°C) on the modulating roles of both cHP and DENV2C on annealing and strand displacement reactions (Figure 2G–I; Tables 3 and 4). Similar to the abovementioned results, we observed that cHP modulates the annealing and strand displacement kinetics even in the presence of 150 mM Na^+ and 1 mM Mg^{2+} ions, (Fig-

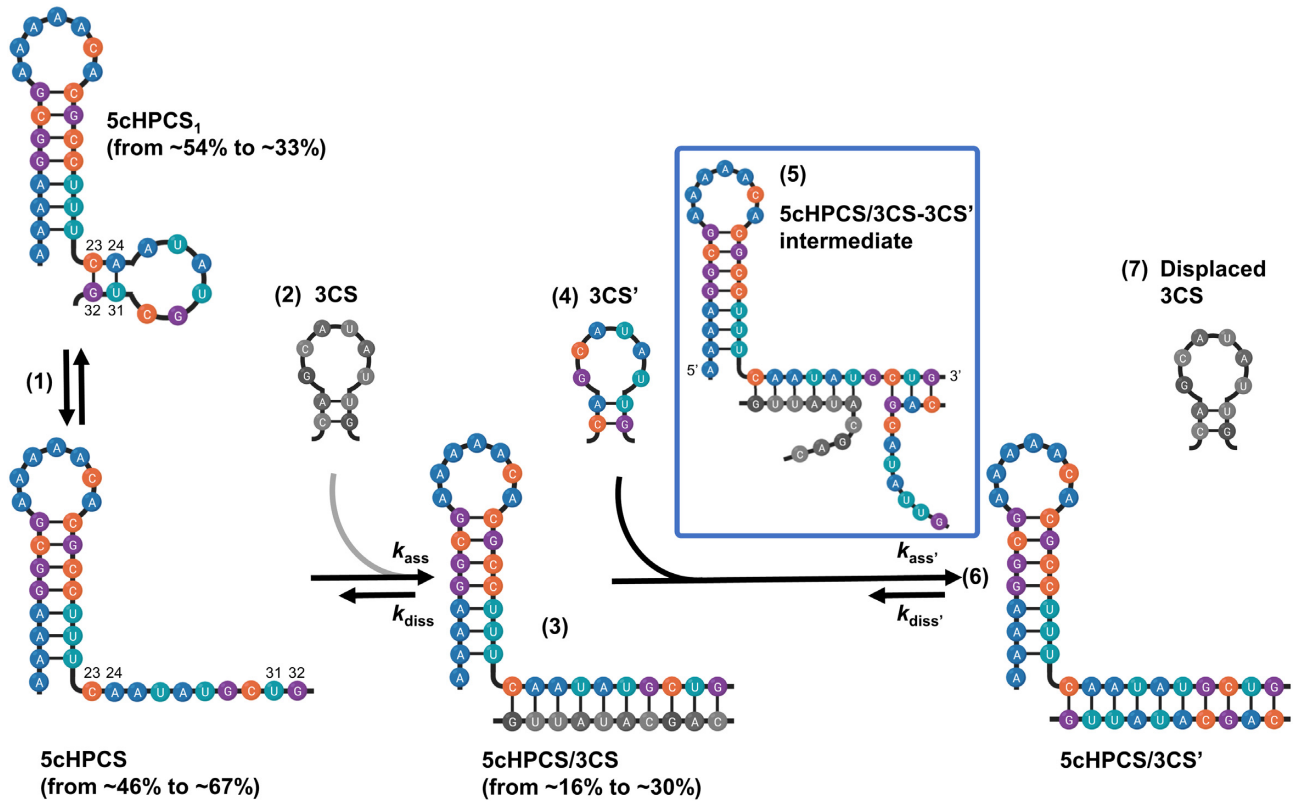

Figure 5. Proposed reaction mechanisms for 5cHPCS/3CS annealing and 5cHPCS/3CS' strand displacement in the presence of DENV2C. The proposed reaction mechanism shows an equilibrium (step 1) between at least two different species of the 5cHPCS (5cHPCS and 5cHPCS$_1$) that originates due to opening of the 5CS hairpin through melting C_{23}-G_{32} and A_{24}-U_{31} base pairs. This melting of base pairs increases from 46% to 67% in the presence of DENV2C that in turn accelerates the annealing reaction in the presence of complementary 3CS (step 2) and leads to higher (up from 16% to 30%) and rapid (2-fold faster) annealed duplex formation (step 3). Population percentages were determined using trFRET at 20°C. DENV2C catalyses the strand displacement reaction in the presence of at least 10-fold molar excess of displacing strand 3CS' (step 4) by destabilizing the 5CS-3CS duplex at the 3′ end of 5cHPCS. This destabilizing of the 3′ edge of the 5CS-3CS duplex lead to nucleation of a transient intermediate triplex (step 5), 5cHPCS/3CS-3CS', that originates from 3′ end of the 5cHPCS (shown in the blue rectangle). The strand displacement reaction leads to the formation of an annealing duplex with 3CS' (step 6) due to the displacement of 3CS (step 7).

Table 3. k_{obs} values obtained from fitting of annealing and strand displacement progress curves at different buffer conditions with equation (1) presented in Figure 2 (Figure 2G and 2H)

		Annealing k_{obs}($\times 10^{-3}$ s^{-1})		Strand displacement $k_{obs'}$($\times 10^{-3}$ s^{-1})	
Buffer composition	DENV2C (2 μM)	5cHPCS/3CS	5CS/3CS	5cHPCS/3CS'	5CS/3CS'
50 mM HEPES, 30 mM NaCl, 0.2 mM $MgCl_2$ @ pH 7.5 (black trace)	–	1.3		No Activity	
	+	3.1		4.1	
50 mM HEPES, 150 mM NaCl, 0.2 mM $MgCl_2$ @ pH 7.5 (red trace)	–	1.1		No Activity	
	+	3.9		4.8	
50 mM HEPES, 30 mM NaCl, 1 mM $MgCl_2$ @ pH 7.5 (green trace)	–	1.4		No Activity	
	+	2.7		1.1	
50 mM HEPES, 150 mM NaCl, 1 mM $MgCl_2$ @ pH 7.5 (blue trace)	–	2.2	4.3	No Activity	No Activity
	+	6.5	9.6	1.8	11.2

Table 4. k_{obs} values obtained from fitting of annealing and strand displacement progress curves at 37°C presented in Figure 2 (in Figure 2I) with equation (1)

	DENV2C (2 μM)	5cHPCS/3CS(3CS')	5CS/3CS(3CS')
Annealing k_{obs} ($\times 10^{-3}$ s^{-1})	–	6.1	13.4
	+	10.4	19.5
Strand displacement $k_{obs'}$ ($\times 10^{-3}$ s^{-1})	–	No Activity	No Activity
	+	11.4	21.5

ure 2G and H; Table 3) as well as at 37°C (Figure 2I; Table 4). Our results also show that DENV2C accelerates annealing and promotes strand displacement despite changes in Mg^{2+} and Na^{+} ions (Figure 2G and H; Table 3), as well as changes in temperature (Figure 2I; Table 4). Furthermore, an increase in Na^{+} (from 30 to 150 mM) and Mg^{2+} (from 0.2 to 1 mM) ions resulted in a ∼2-fold increase and a ∼2-fold decrease in the annealing and strand displacement rates of 5cHPCS/3CS, respectively. This increase in the annealing reaction rate can be attributed to an increase in the screening of the negatively charged ORN due to the presence of positively charged ions, thus accelerating duplex formation (68,69). In addition, the higher concentration of Mg^{2+} ions may lead to the stabilization of the 5cHPCS/3CS duplexes, resulting in slower strand displacement of 3CS by 3CS' (68,70). Our experiment used short but relevant RNA sequences, providing mechanistic information about how DENV2C works as a chaperone during RNA rearrangement via annealing and strand displacement. In the future, it will be important to use longer ORNs to gain a more comprehensive understanding of the RNA chaperone role of DENV2C in genomic rearrangement. Our strand displacement reactions were also done using an excess of 3CS instead of 5CS to maintain the duplex state of 5cHPCS/3CS before and after strand displacement. Be that as it may, our findings about the modulating role of cHP and DENV2C on annealing and strand displacement should hold true in either experimental condition. Future work on genome rearrangements during (−) RNA synthesis can use 5CS instead of 3CS for 5cHPCS/3CS strand displacement.

Previous work on DENVC showed that the protein had RNA chaperoning properties as it facilitates typical hammerhead structure formation (22). DENVC was necessary for hammerhead ribozyme activity, promoting annealing of the substrate RNA to the ribozyme and the subsequent dissociation of the cleaved RNA products from the ribozyme (22). Thus, as an RNA chaperone, DENV2C is hypothesized to be involved in essential genome rearrangement events and yet, the mechanism by which DENV2C rearranges the viral genome during RNA synthesis is one of the most obscure steps of the DENV life cycle. In this paper, we provide (i) mechanistic insights into the stabilization of the 5′-3′ panhandle genome structure by cHP and (ii) how DENV2C modulates the function of cHP during 5CS-3CS annealing and strand displacement. To our knowledge, this is the first demonstration of DENV2C chaperoning strand displacement from an annealed duplex, using genomic RNA sequences. Our results corroborate well with previous work involving the hammerhead ribozyme assay, where conserved sequences involved in circularization (5UAR, 5CS, 3UAR and 3CS) were incorporated into hammerhead ribozymes and their substrates to observe annealing and dissociation (22). In both studies, DENVC was required for RNA strand displacement activity. In addition, our results shed light on the kinetics and mechanism behind the RNA chaperoning property of DENV2C.

Other viral proteins also have RNA regulating properties. NS3 helicase is shown to have helicase activity, facilitating RNA unwinding and thus RNA synthesis and is also able to promote annealing between complementary RNA (71). However, NS3 is not considered to be an RNA chaperone because it is unable to refold RNA with a complex secondary structure. This process, tested via a hammerhead ribozyme assay, involves both annealing and dissociation of RNA (22). NS3 helicase activity is ATP-dependent, whereas its annealing activity is ATP-independent (71). Thus, it is likely that NS3 can fold and refold complex RNA structures and take part in strand displacement, based on ATP availability. Be that as it may, the only viral protein with strong RNA chaperone activities is shown to be DENVC (22), and it is likely that DENVC would play a key role in annealing and strand displacement during genome rearrangements. While out of the scope of this paper, which focuses on DENV2C as an ATP-independent RNA chaperone, it would be interesting to study the effect and ATP-dependence of NS3 in DENV2C-promoted RNA rearrangement.

The strand displacement capabilities of DENV2C are critical for genomic RNA rearrangement in DENV replication and RNA packaging as well as in facilitating rearrangement between various DENV genotypes and subtypes to increase viral variability. Moreover, delineation of RNA structures in the presence of RNA chaperones like DENV2C serves to broaden our understanding of the mechanisms virus use to reproduce and to subvert or evade the host antiviral response, and allows for the focused development of vaccines and antiviral therapies.

SUPPLEMENTARY DATA

Supplementary Data are available at NAR Online.

FUNDING

National Research Foundation Singapore [NRF-CRP19-2017-03–00]; Integrative Sciences and Engineering Programme under the NUS Graduate School (to X.E.Y.). Funding for open access charge: Thorsten Wohland [NRF-CRP19-2017-03–00].
Conflict of interest statement. None declared.

REFERENCES

1. Chambers,T.J., Hahn,C.S., Galler,R. and Rice,C.M. (1990) Flavivirus genome organization, expression, and replication. *Genome*, **44**, 649–688.
2. Gubler,D.J. (1998) Dengue and dengue hemorrhagic fever. *Clin. Microbiol. Rev.*, **11**, 480–496.
3. Lindenbach,B.D. and Knipe,D. M. (2001) Flaviviridae: the viruses and their replication, **1**, 991–1041.
4. Alvarez,D.E., De Lella Ezcurra,A.L., Fucito,S. and Gamarnik,A.V. (2005) Role of RNA structures present at the 3′UTR of dengue virus on translation, RNA synthesis, and viral replication. *Virology*, **339**, 200–212.
5. Alvarez,D.E., Lodeiro,M.F., Ludueña,S.J., Lía,I., Gamarnik,A.V, Lodeiro,F. and Luduen,S.J. (2005) Long-range RNA-RNA interactions circularize the dengue virus genome long-range RNA-RNA interactions circularize the dengue virus genome. *J. Virol.*, **79**, 6631–6643.
6. Zeng,L., Falgout,B. and Markoff,L. (1998) Identification of specific nucleotide sequences within the conserved 3′-SL in the dengue type 2 virus genome required for replication. *J. Virol.*, **72**, 7510–7522.
7. Chiu,W.-W., Kinney,R.M. and Dreher,T.W. (2005) Control of translation by the 5′- and 3′-terminal regions of the dengue virus genome. *J. Virol.*, **79**, 8303–8315.

8. Khromykh,A.A., Meka,H., Guyatt,K.J. and Westaway,E.G. (2001) Essential role of cyclization sequences in flavivirus RNA replication. *J. Virol.*, **75**, 6719–6728.
9. Friebe,P. and Harris,E. (2010) Interplay of RNA elements in the dengue virus 5′ and 3′ ends required for viral RNA replication. *J. Virol.*, **84**, 6103–6118.
10. Friebe,P., Shi,P.-Y. and Harris,E. (2011) The 5′ and 3′ downstream aug region elements are required for mosquito-borne flavivirus RNA replication. *J. Virol.*, **85**, 1900–1905.
11. Alvarez,D.E., Filomatori,C.V. and Gamarnik,A.V. (2008) Functional analysis of dengue virus cyclization sequences located at the 5′ and 3′UTRs. *Virology*, **375**, 223–235.
12. Liu,Z.-Y., Li,X.-F., Jiang,T., Deng,Y.-Q., Zhao,H., Wang,H.-J., Ye,Q., Zhu,S.-Y., Qiu,Y., Zhou,X. *et al.* (2013) Novel cis-acting element within the capsid-coding region enhances flavivirus viral-RNA replication by regulating genome cyclization. *J. Virol.*, **87**, 6804–6818.
13. de Borba,L., Villordo,S.M., Marsico,F.L., Carballeda,J.M., Filomatori,C.V., Gebhard,L.G., Pallarés,H.M., Lequime,S., Lambrechts,L., Vargas,I.S. *et al.* (2019) RNA structure duplication in the dengue virus 3′ UTR: redundancy or host specificity? *MBio*, **10**, e02506-18.
14. Clyde,K., Barrera,J. and Harris,E. (2008) The capsid-coding region hairpin element (cHP) is a critical determinant of dengue virus and West Nile virus RNA synthesis. *Virology*, **379**, 314–323.
15. Clyde,K. and Harris,E. (2006) RNA secondary structure in the coding region of dengue virus type 2 directs translation start codon selection and is required for viral replication. *J. Virol.*, **80**, 2170–2182.
16. Polacek,C., Foley,J.E. and Harris,E. (2009) Conformational changes in the solution structure of the dengue virus 5′ end in the presence and absence of the 3′ untranslated region. *J. Virol.*, **83**, 1161–1166.
17. Dethoff,E.A., Boerneke,M.A., Gokhale,N.S., Muhire,B.M., Martin,D.P., Sacco,M.T., McFadden,M.J., Weinstein,J.B., Messer,W.B., Horner,S.M. *et al.* (2018) Pervasive tertiary structure in the dengue virus RNA genome. *Proc. Natl. Acad. Sci. USA*, **115**, 11513–11518.
18. Villordo,S.M., Alvarez,D.E. and Gamarnik,A.V. (2010) A balance between circular and linear forms of the dengue virus genome is crucial for viral replication. *RNA*, **16**, 2325–2335.
19. Johansson,M., Brooks,A.J., Jans,D.A. and Vasudevan,S.G. (2001) A small region of the dengue virus-encoded RNA-dependent RNA polymerase, NS5, confers interaction with both the nuclear transport receptor importin-β and the viral helicase, NS3. *J. Gen. Virol.*, **82**, 735–745.
20. Takahashi,H., Takahashi,C., Moreland,N.J., Chang,Y.T., Sawasaki,T., Ryo,A., Vasudevan,S.G., Suzuki,Y. and Yamamoto,N. (2012) Establishment of a robust dengue virus NS3-NS5 binding assay for identification of protein-protein interaction inhibitors. *Antiviral Res.*, **96**, 305–314.
21. Yong,X.E., Raghuvamsi,P.V., Anand,G.S., Wohland,T. and Sharma,K.K. (2021) Dengue virus strain 2 capsid protein switches the annealing pathway and reduces intrinsic dynamics of the conserved 5′ untranslated region. *RNA Biol.*, **18**, 718–731.
22. Pong,W.L., Huang,Z.S., Teoh,P.G., Wang,C.C. and Wu,H.N. (2011) RNA binding property and RNA chaperone activity of dengue virus core protein and other viral RNA-interacting proteins. *FEBS Lett.*, **585**, 2575–2581.
23. Herschlag,D. (1995) RNA chaperones and the RNA folding problem. *J. Biol. Chem.*, **270**, 20871–20874.
24. Ivanyi-Nagy,R., Lavergne,J.P., Gabus,C., Ficheux,D. and Darlix,J.L. (2008) RNA chaperoning and intrinsic disorder in the core proteins of Flaviviridae. *Nucleic Acids Res.*, **36**, 712–725.
25. Ma,L., Jones,C.T., Groesch,T.D., Kuhn,R.J. and Post,C.B. (2004) Solution structure of dengue virus capsid protein reveals another fold. *Proc. Natl. Acad. Sci. USA*, **101**, 3414–3419.
26. Tompa,P. and Csermely,P. (2004) The role of structural disorder in the function of RNA and protein chaperones. *FASEB J.*, **18**, 1169–1175.
27. Boon,P.L.S., Saw,W.G., Lim,X.X., Raghuvamsi,P.V., Huber,R.G., Marzinek,J.K., Holdbrook,D.A., Anand,G.S., Grüber,G. and Bond,P.J. (2018) Partial intrinsic disorder governs the dengue capsid protein conformational ensemble. *ACS Chem. Biol.*, **13**, 1621–1630.
28. Kuhn,R.J., Zhang,W., Rossmann,M.G., Pletnev,S.V., Corver,J., Lenches,E., Jones,C.T., Mukhopadhyay,S., Chipman,P.R., Strauss,E.G. *et al.* (2002) Structure of dengue virus: Implications for flavivirus organization, maturation, and fusion. *Cell*, **108**, 717–725.
29. Sangiambut,S., Keelapang,P., Aaskov,J., Puttikhunt,C., Kasinrerk,W., Malasit,P. and Sittisombut,N. (2008) Multiple regions in dengue virus capsid protein contribute to nuclear localization during virus infection. *J. Gen. Virol.*, **89**, 1254–1264.
30. Boudier,C., Storchak,R., Sharma,K.K., Didier,P., Follenius-Wund,A., Muller,S., Darlix,J.L. and Mély,Y. (2010) The Mechanism of HIV-1 Tat-Directed Nucleic Acid Annealing Supports its Role in Reverse Transcription. *J. Mol. Biol.*, **400**, 487–501.
31. Ramalanjaona,N., Rocquigny,H., Millet,A., Ficheux,D., Darlix,J.-L. and Mély,Y. (2007) Investigating the mechanism of the nucleocapsid protein chaperoning of the second strand transfer during HIV-1 DNA synthesis. *J. Mol. Biol.*, **374**, 1041–1053.
32. Godet,J., Rocquigny,H., Raja,C., Glasser,N., Ficheux,D., Darlix,J.-L. and Mély,Y. (2006) During the early phase of HIV-1 DNA synthesis, nucleocapsid protein directs hybridization of the TAR complementary sequences via the ends of their double-stranded stem. *J. Mol. Biol.*, **356**, 1180–1192.
33. Vo,M.N., Barany,G., Rouzina,I. and Musier-Forsyth,K. (2009) HIV-1 nucleocapsid protein switches the pathway of transactivation response element RNA/DNA annealing from loop-loop 'kissing' to 'zipper'. *J. Mol. Biol.*, **386**, 789–801.
34. Sharma,K.K., Didier,P., Darlix,J.L., de Rocquigny,H., Bensikaddour,H., Lavergne,J.P., Pénin,F., Lessinger,J.M. and Mély,Y. (2010) Kinetic analysis of the nucleic acid chaperone activity of the hepatitis C virus core protein. *Nucleic Acids Res.*, **38**, 3632–3642.
35. Sharma,K.K., De Rocquigny,H., Darlix,J.L., Lavergne,J.P., Pénin,F., Lessinger,J.M. and Mély,Y. (2012) Analysis of the RNA chaperoning activity of the hepatitis C virus core protein on the conserved 3′X region of the viral genome. *Nucleic Acids Res.*, **40**, 2540–2553.
36. Sharma,K.K., Przybilla,F., Restle,T., Boudier,C., Godet,J. and Mély,Y. (2015) Reverse transcriptase in action: FRET-based assay for monitoring flipping and polymerase activity in real time. *Anal. Chem.*, **87**, 7690–7697.
37. Sharma,K.K., Przybilla,F., Restle,T., Godet,J. and Mély,Y. (2016) FRET-based assay to screen inhibitors of HIV-1 reverse transcriptase and nucleocapsid protein. *Nucleic Acids Res.*, **44**, e74.
38. Kuzmič,P. (1996) Program DYNAFIT for the analysis of enzyme kinetic data: application to HIV proteinase. *Anal. Biochem.*, **237**, 260–273.
39. Semrad,K., Green,R. and Schroeder,R. (2004) RNA chaperone activity of large ribosomal subunit proteins from Escherichia coli. *RNA*, **10**, 1855–1860.
40. Cristofari,G., Ivanyi-Nagy,R., Gabus,C., Boulant,S., Lavergne,J.P., Penin,F. and Darlix,J.L. (2004) The hepatitis C virus core protein is a potent nucleic acid chaperone that directs dimerization of the viral (+) strand RNA in vitro. *Nucleic Acids Res.*, **32**, 2623–2631.
41. Rajkowitsch,L., Chen,D., Stampfl,S., Semrad,K., Waldsich,C., Mayer,O., Jantsch,M.F., Konrat,R., Bläsi,U. and Schroeder,R. (2007) RNA chaperones, RNA annealers and RNA helicases. *RNA Biol.*, **4**, 118–130.
42. McKnight,K.L. and Lemon,S.M. (1996) Capsid coding sequence is required for efficient replication of human rhinovirus 14 RNA. *J. Virol.*, **70**, 1941–1952.
43. Mcknight,K.L. and Lemon,S.M. (1998) The rhinovirus type 14 genome contains an internally located RNA structure that is required for viral replication. *RNA*, **4**, 1569–1584.
44. Gerber,K., Wimmer,E. and Paul,A.V. (2001) Biochemical and genetic studies of the initiation of human rhinovirus 2 RNA replication: identification of a cis-replicating element in the coding sequence of 2Apro. *J. Virol.*, **75**, 10979–10990.
45. Goodfellow,I., Chaudhry,Y., Richardson,A., Meredith,J., Almond,J.W., Barclay,W. and Evans,D.J. (2000) Identification of a cis-acting replication element within the poliovirus coding region. *J. Virol.*, **74**, 4590–4600.
46. van Ooij,M.J.M., Vogt,D.A., Paul,A., Castro,C., Kuijpers,J., van Kuppeveld,F.J.M., Cameron,C.E., Wimmer,E., Andino,R. and Melchers,W.J.G. (2006) Structural and functional characterization of the coxsackievirus B3 CRE (2C): role of CRE (2C) in negative-and positive-strand RNA synthesis. *J. Gen. Virol.*, **87**, 103–113.
47. Lobert,P.E., Escriou,N., Ruelle,J. and Michiels,T. (1999) A coding RNA sequence acts as a replication signal in cardioviruses. *Proc. Natl. Acad. Sci. USA*, **96**, 11560–11565.

48. Murray,K.E. and Barton,D.J. (2003) Poliovirus CRE-dependent VPg uridylylation is required for positive-strand RNA synthesis but not for negative-strand RNA synthesis. *J. Virol.*, **77**, 4739–4750.
49. Yang,Y., Rijnbrand,R., McKnight,K.L., Wimmer,E., Paul,A., Martin,A. and Lemon,S.M. (2002) Sequence requirements for Viral RNA replication and VPg uridylylation directed by the internal cis-acting replication element (cre) of human rhinovirus type 14. *J. Virol.*, **76**, 7485–7494.
50. You,S., Stump,D.D., Branch,A.D. and Rice,C.M. (2004) A cis-acting replication element in the sequence encoding the NS5B RNA-dependent RNA polymerase is required for hepatitis C virus RNA replication. *J. Virol.*, **78**, 1352–1366.
51. Friebe,P., Boudet,J., Simorre,J.-P. and Bartenschlager,R. (2005) Kissing-loop interaction in the 3′ end of the hepatitis C virus genome essential for RNA replication. *J. Virol.*, **79**, 380–392.
52. Holden,K.L. and Harris,E. (2004) Enhancement of dengue virus translation: Role of the 3′ untranslated region and the terminal 3′ stem-loop domain. *Virology*, **329**, 119–133.
53. Holden,K.L., Stein,D.A., Pierson,T.C., Ahmed,A.A., Clyde,K., Iversen,P.L. and Harris,E. (2006) Inhibition of dengue virus translation and RNA synthesis by a morpholino oligomer targeted to the top of the terminal 3′ stem-loop structure. *Virology*, **344**, 439–452.
54. Tilgner,M., Deas,T.S. and Shi,P.-Y. (2005) The flavivirus-conserved penta-nucleotide in the 3′ stem-loop of the West Nile virus genome requires a specific sequence and structure for RNA synthesis, but not for viral translation. *Virology*, **331**, 375–386.
55. You,S., Falgout,B., Markoff,L. and Padmanabhan,R. (2001) In vitro RNA synthesis from exogenous dengue viral RNA templates requires long range interactions between 5′- and 3′-terminal regions that influence RNA structure. *J. Biol. Chem.*, **276**, 15581–15591.
56. Filomatori,C.V., Lodeiro,M.F., Alvarez,D.E., Samsa,M.M., Pietrasanta,L. and Gamarnik,A.V. (2006) A 5′ RNA element promotes dengue virus RNA synthesis on a circular genome. *Genes Dev.*, **20**, 2238–2249.
57. Nomaguchi,M., Ackermann,M., Yon,C., You,S. and Padmanabhan,R. (2003) De novo synthesis of negative-strand RNA by Dengue virus RNA-dependent RNA polymerase in vitro: nucleotide, primer, and template parameters. *J. Virol.*, **77**, 8831–8842.
58. Nomaguchi,M., Teramoto,T., Yu,L., Markoff,L. and Padmanabhan,R. (2004) Requirements for West Nile virus (−)- and (+)-strand subgenomic RNA synthesis in vitro by the viral RNA-dependent RNA polymerase expressed in Escherichia coli. *J. Biol. Chem.*, **279**, 12141–12151.
59. You,S. and Padmanabhan,R. (1999) A novel in vitro replication system for Dengue virus. Initiation of RNA synthesis at the 3′-end of exogenous viral RNA templates requires 5′- and 3′-terminal complementary sequence motifs of the viral RNA. *J. Biol. Chem.*, **274**, 33714–33722.
60. Karnib,H., Nadeem,M.F., Humbert,N., Sharma,K.K., Grytsyk,N., Tisné,C., Boutant,E., Lequeu,T., Réal,E., Boudier,C. *et al.* (2020) The nucleic acid chaperone activity of the HIV-1 Gag polyprotein is boosted by its cellular partner RPL7: a kinetic study. *Nucleic Acids Res.*, **48**, 9218–9234.
61. Urbaneja,M.A., Wu,M., Casas-Finet,J.R. and Karpel,R.L. (2002) HIV-1 nucleocapsid protein as a nucleic acid chaperone: spectroscopic study of its helix-destabilizing properties, structural binding specificity, and annealing activity. *J. Mol. Biol.*, **318**, 749–764.
62. Ermolenko,D.N. and Makhatadze,G.I. (2002) Bacterial cold-shock proteins. *Cell. Mol. Life Sci.*, **59**, 1902–1913.
63. Sasaki,K., Kim,M.H. and Imai,R. (2007) Arabidopsis COLD SHOCK DOMAIN PROTEIN2 is a RNA chaperone that is regulated by cold and developmental signals. *Biochem. Biophys. Res. Commun.*, **364**, 633–638.
64. Kang,H., Park,S.J. and Kwak,K.J. (2013) Plant RNA chaperones in stress response. *Trends Plant Sci.*, **18**, 100–106.
65. Jiang,W., Hou,Y. and Inouye,M. (1997) CspA, the major cold-shock protein of Escherichia coli, is an RNA chaperone. *J. Biol. Chem.*, **272**, 196–202.
66. Schroeder,R., Grossberger,R., Pichler,A. and Waldsich,C. (2002) RNA folding in vivo. *Curr. Opin. Struct. Biol.*, **12**, 296–300.
67. Doetsch,M., Schroeder,R. and Fürtig,B. (2011) Transient RNA-protein interactions in RNA folding. *FEBS J.*, **278**, 1634–1642.
68. Doetsch,M., Fürtig,B., Gstrein,T., Stampfl,S. and Schroeder,R. (2011) The RNA annealing mechanism of the HIV-1 Tat peptide: conversion of the RNA into an annealing-competent conformation. *Nucleic Acids Res.*, **39**, 4405–4418.
69. Lapadat-tapolsky,M., Pernelle,C., Borie,C. and Darlix,J. (1995) Analysis of the nucleic acid annealing activites of nucleocapsid protein from HIV-1. *Nucleic Acids Res.*, **23**, 2434–2441.
70. Misra,V.K. and Draper,D.E. (1998) On the role of magnesium ions in RNA stability. *Biopolymers*, **48**, 113–135.
71. Gebhard,L.G., Kaufman,S.B. and Gamarnik,A.V. (2012) Novel ATP-independent RNA annealing activity of the dengue virus NS3 helicase. *PLoS One*, **7**, 27–29.